AEROELASTIC BEHAVIOR OF TYPICAL SECTIONS WITH STRUCTURAL NONLINEARITY IN TRANSONIC FLOW

Elizangela Camilo and João Luiz F. Azevedo
Instituto de Aeronáutica e Espaço, CTA/IAE/ALA, São José dos Campos, SP, 12228-903, BRAZIL

Keywords: *Aeroelasticity, transonic flow, structural nonlinearity, LCO, flutter boundary.*

Abstract

The paper is concerned with aeroelastic analyses of an airfoil system in which both aerodynamic and structural nonlinearities are considered. Here, structural dynamics is treated in terms of polynomial nonlinearities. The work aims to investigate effects of initial incidence changes in the aeroelastic equations of typical sections in transonic flows. Major interest is in verifying how the different initial incidences affect the transonic aeroelastic behavior with concentrated structural nonlinearities. A non-zero mean angle-of-attack position of the torsional spring is incorporated into the model to analyze the characteristic of system equilibrium position for a range of parameters. An Euler CFD code based on a finite volume discretization on unstructured grid is used for the unsteady aerodynamic loading assessment. The results are particularly concerned with the investigation of nonlinear effects for transonic flow over a NACA 0012 airfoil-based typical section. The investigation considers both time histories of the aeroelastic response as well as flutter speed boundary analyses.

1 Introduction

Nonlinear aeroelasticity is a multidisciplinary field, that is very important in aeronautics and aerospace engineering. Aeroelasticity can be defined as the science which studies the mutual interaction between aerodynamic and dynamic forces [1]. The influence of nonlinearities on modern aircraft is becoming increasingly important and the need for more accurate predictive tools grows stronger.

The nonlinearities in aeroelastic analyses are divided into aerodynamic and structural ones. In this paper, the aerodynamic nonlinearities arise from the presence of shock waves in transonic flows. Structural nonlinearities can be classified as distributed or concentrated. The distributed nonlinearities are spread over the entire structure and can manifest themselves through complex material behavior, by aging effects, and due to faulty joints, junctions, or links. The concentrated nonlinearities are those acting locally, being basically assumed for simplified structural models [2].

Computational aeroelasticity is a relatively new field emphasizing those types of aeroelastic problems where loads based on CFD methods, which can be both unsteady and nonlinear, are used. A significant amount of effort has been devoted towards the numerical solution of transonic aeroelastic phenomena, not only in the prediction of transonic dip effects [3, 4, 5], but also towards that of limit cycle oscillations (LCOs). Euler and Navier–Stokes schemes have been coupled with structural models [6]. Studies with concentrated nonlinearities have revealed significant effects on the aeroelastic stability, allowing the presence of chaotic motion and limit cycle oscillations below the flutter speed [7].

The methodology here presented is applied to obtain the time domain aeroelastic responses for an airfoil moving in pitch and plunge in the transonic regime [6, 8]. The aim of this paper

is to investigate the nonlinear behavior of typical airfoil sections with structural and aerodynamic nonlinearities. The modeling methodology is based on coupling typical section motion equations to an Euler unsteady CFD code to obtain time-marching aeroelastic responses through the fourth-order Runge-Kutta scheme. The present investigation of the time–marching tool is a result of the increased demand for nonlinear aeroelastic parameters analysis that can influence dynamic system behavior. Previous work have performed flutter boundaries calculations where time-marching solutions are compared with those from a computationally more attractive Hopf bifurcation analysis [9]. An Euler model is used for the fuid, while the structure is represented as a NACA 0012 airfoil with nonlinear torsional stiffness.

Time-marching analysis of nonlinear aeroelasticity has been performed for detailed motion characteristics [7, 10]. Different initial incidence effects in the aeroelastic responses with linear and nonlinear structural model have been started in the previous work [10]. The aim of this paper is to follow the investigation of nonlinear behavior considering different initial incidences with concentrated structural nonlinearities in the model. Also, this work intends to incoporate a non-zero mean angle-of-attack position of the torsional spring into the model to verify how system parameters can affect the equilibrium solutions of the transonic aeroelastic behavior by looking time histories development. Such analysis is based on a Hopf point prediction to calculate direct flutter speed is an equilibrium position of the system which satisfies additional constraints. Thus, characterizing the equilibrium solution space of a system for a wide range of parameter is important [3].

The modeling methodology is based on coupling typical section motion equations to an Euler unsteady CFD code to obtain time–marching aeroelastic responses through the fourth-order Runge–Kutta scheme. In order to solve the aerodynamic problem, the Euler equations are integrated by a finite volume discretization on unstructured grids. The development of the present CFD tool is the evolution of the work and projects performed by CTA/IAE [11, 12, 13, 14]. Nevertheless, this CFD tool has been developed for the unsteady aerodynamic and aeroelastic applications in the work of [9, 12, 15, 16, 17]. Concentrated structural nonlinearities are introduced into the model. In this way, torsional nonlinearities, described by polynomial functions, have been considered. The results are presented in terms of time-marching analyses, where time histories of the aeroelastic response are considered. To illustrate the performance of the time-marching solver, complete flutter boundaries for a NACA 0012 airfoil with torsional structural nonlinearity is performed. The flutter boundary results are compared with the Hopf bifurcation predictions obtained in previous work.

2 Aerodynamic Model

In the present study, the flow is assumed to be governed by the two-dimensional, time-dependent Euler equations, which may be written in conservative form and Cartesian coordinates as

$$\frac{\partial}{\partial t}\int\int_{\mathbf{V}} \mathbf{Q}dxdy + \int_{\mathbf{S}} (\mathbf{E}dy - \mathbf{F}dx) = 0, \qquad (1)$$

where **V** represents the area of the control volume and **S** is its boundary, **Q** is the vector of conserved quantities and the inviscid flux vectors, **E** and **F**, are given by

$$\mathbf{Q} = \begin{bmatrix} \rho \\ \rho u \\ \rho v \\ e \end{bmatrix}, \qquad \mathbf{E} = \begin{bmatrix} \rho U \\ \rho u U + p \\ \rho v U \\ (e+p)U + x_t p \end{bmatrix},$$
$$\mathbf{F} = \begin{bmatrix} \rho V \\ \rho V u \\ \rho V v + p \\ (e+p)V + y_t p \end{bmatrix}, \qquad (2)$$

where ρ, u, v, p and e are density, Cartesian components of the velocity, pressure, and specific energy, respectively. U and V are contravariant velocity components, defined as

$$U = u - x_t \ , \qquad V = v - y_t \ , \qquad (3)$$

where x_t and y_t represents the Cartesian velocity components of the mesh.

The Euler equations can be rewritten for each *i-th* control volume as

$$\frac{\partial}{\partial t}(V_i \mathbf{Q}_i) + \int_{S_i} (\mathbf{E}dy - \mathbf{F}dx) = 0 \,. \qquad (4)$$

The 2-D Euler equations are discretized by a finite volume procedure in an unstructured mesh. The equations are discretized in space by a centered scheme, together with added artificial dissipation terms. The artificial dissipation operator, D_i, can be written as

$$D_i = d^2(\mathbf{Q}_i) - d^4(\mathbf{Q}_i) \,, \qquad (5)$$

where $d^2(\mathbf{Q}_i)$ represents the contribution of the undivided Laplacian operator, and $d^4(\mathbf{Q}_i)$ is the contribution of the biharmonic operator [18]. The biharmonic operator is responsible for providing the background dissipation to damp high frequency uncoupled error modes and the undivided Laplacian artificial dissipation operator prevents oscillations near shock waves. The Euler solver is integrated in time by a second-order accurate, 5-stage, explicit, Runge-Kutta time-stepping scheme, as presented in [15].

3 Aeroelastic Equations

The physical model considered in the present work is a typical section with pitch and plunge degrees of freedom and free of mechanical friction [1].

$$m\ddot{h} - S_\alpha \ddot{\alpha} + K_h h = -L, \qquad (6)$$

$$-S_\alpha \ddot{h} + I_\alpha \ddot{\alpha} + K_\alpha(\alpha - \alpha_0) = M_{ea}. \qquad (7)$$

where h is the plunge linear displacement and α is the incidence, or pitch angular displacement. S_α is the static moment about elastic axis, K_w and K_α are translational and torsional stiffness about elastic axis, respectively. In the present formulation α_0 is the mean initial angle-of-attack. Here the left-hand-side terms represent a linear structural model approximation for the vertical displacement and pitch coordinates. The right-hand-side terms represent the aerodynamic loading terms, which are obtained from CFD code.

The equations of motion of this aeroelastic system, with a linear structure, can be rewritten in the form

$$\frac{d\mathbf{w}_s}{dt} = \mathbf{R}_s \,, \qquad (8)$$

where

$$\mathbf{R}_s = \begin{bmatrix} 1 & 0 & 0 & 0 \\ 0 & 1 & 0 & \frac{1}{2}x_\alpha \\ 0 & 0 & 1 & 0 \\ 0 & x_\alpha & 0 & \frac{1}{2}r_\alpha^2 \end{bmatrix}^{-1} \left\{ \begin{bmatrix} 0 \\ (2/\mu_s\pi)C_l \\ 0 \\ (4/\mu_s\pi)C_m \end{bmatrix} - \begin{bmatrix} 0 & -1 & 0 & 0 \\ (2\omega_R/\bar{U})^2 & 0 & 0 & 0 \\ 0 & 0 & 0 & -1 \\ 0 & 0 & 2r_\alpha^2/(\bar{U})^2 & 0 \end{bmatrix} \mathbf{w}_s \right\} \qquad (9)$$

and $\mathbf{w}_s = [h, \dot{h}, \alpha - \alpha_0, \dot{\alpha}]^T$. Here, $r_\alpha = \sqrt{(I_\alpha/m)}$ is the radius of gyration defined in terms of the pitch moment of inertia I_α and the airfoil mass per unit span m, x_α is the offset between the center of mass and the elastic axis, $\mu_s = m/\pi\rho_\infty b^2$ is the airfoil-to-fluid mass ratio defined in terms of the fluid freestream density ρ_∞ and the semi-chord, b. Moreover, $\omega_R = \frac{\omega_h}{\omega_\alpha}$ is the ratio of the natural frequencies of plunging (ω_h) and pitching (ω_α), $\bar{U} = \frac{U_\infty}{b\omega_\alpha}$ is the reduced velocity defined in terms of the fluid freestream velocity U_∞, and C_l and C_m are the lift and moment coefficients about the elastic axis, respectively.

The fouth–order Runge–Kutta time stepping scheme is used for the time marching aeroelastic analyses. Time integration of the coupled fluid–structure equations of motion is incorporated within the CFD Euler code as follows [10]:

1. Starting from a converged steady–state solution of the flow over the rigid airfoil, perform a time step of the Euler equations in the initial position of the airfoil and calculate values for C_l and C_m;

2. The new position and velocity of the airfoil are obtained by solving the dynamic equations of motion, Eq. (8), using the a fourth–order Runge–Kutta time–stepping scheme;

3. The aerodynamic mesh is moved, and the mesh nodal velocities are calculated, in or-

der to accommodate the new position and velocity of the airfoil;

4. The unsteady Euler equations are resolved in order to obtain new aerodynamic coefficients;

5. Then, one can return to step (2) to calculate new position and velocity of the airfoil, and the process is repeated.

4 Torsional Structural Nonlinearity

Several classes of nonlinear stiffness contributions have been studied in papers treating the open-loop dynamics of the aeroelastic system [2]. In this work, the linear torsional moment function is replaced by the nonlinear function

$$\bar{M}(\alpha) = \bar{K}_\alpha \alpha = K_\alpha f(\alpha) \,, \qquad (10)$$

where K_α is considered as a global stiffness. The functional form of $f(\alpha)$ can be expressed as a polynomial nonlinearity for restoring torsion

$$f(\alpha) = f_{\alpha_0} + f_{\alpha_1}\alpha + f_{\alpha_2}\alpha^2 + \ldots + f_{\alpha_n}\alpha^n \,. \quad (11)$$

Again, non-zero mean angle-of-attack α_0 position of the torsional spring is incorporated into the nonlinear model

$$\bar{M}(\alpha - \alpha_0) = \bar{K}_\alpha(\alpha - \alpha_0) = K_\alpha f(\alpha - \alpha_0) \quad (12)$$

5 Time-Marching and Flutter Boundaries Analyses

5.1 Effect of Initial Incidence

Time-marching and flutter boundaries results have been obtained with the linear and nonlinear structural models. The Hopf bifurcation analyses [4] were used to calculate airfoil flutter boundaries and the results are showed in comparison with time-marching calculations for the same flight conditions, as in [9].

The results for the time marching method have been studied through the time histories of the solution. The parameters for the structural model are given in Table 1. The results were calculated by first computing a converged steady flow solution at airfoil initial incidence about the elastic axis. The steady Euler solution was determined using the steady portion of the original unsteady Euler solver. Then, the coupled computational fluid dynamic (CFD) and computational structural dynamics (CSD) method to the two-dimensional typical section was performed. It consists of a NACA0012 airfoil.

Table 1 Structural model parameters.

Parameter	Value
r_α	0.539
x_α	-0.2
ω_R	0.343
μ_s	100.0
x_{ea}	-0.1
y_{ea}	0.0

Different initial incidences have been performed in order to study the effects in the transonic aeroelastic behavior for both cases, linear structural model and torsional nonlinear structural model analyses. The case analyzed corresponds to structural model parameters in the Table 1. First, the analysis are evaluated with zero medium angle-of-attack of torsional spring position, *i.e.*, $\alpha_0 = 0$.

Aeroelastic responses with linear structural model at fixed $M_\infty = 0.86$ and $\bar{U} = 3.36$ are obtained, where four initial incidences have been considered and given by 0.3°, 0.5°, 1.0° and -1.0°. The time history for the initial incidence of 0.3° is presented in Fig. 1. The system exhibits oscillations with slightly decreasing amplitudes. Such behavior is consistent with the fact that this point has been considered closer to flutter point. One can observe that the system exhibits oscillations with incidences between 0.1° and -0.1°.

The system also exhibits oscillations with slightly decreasing amplitudes when initial incidences of 0.5°, 1.0° and -1.0° are used, as shown in Figs. 2, 3 and 4, respectively. For initial incidence of 0.5°, the system exhibits oscillations with incidences between 0.2° and -0.2°, as

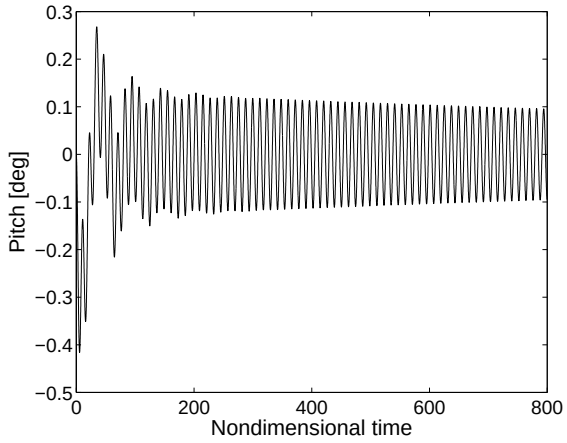

Fig. 1 Time history for linear structural model at $M = 0.86$, $\bar{U} = 3.36$ and 0.3° initial incidence.

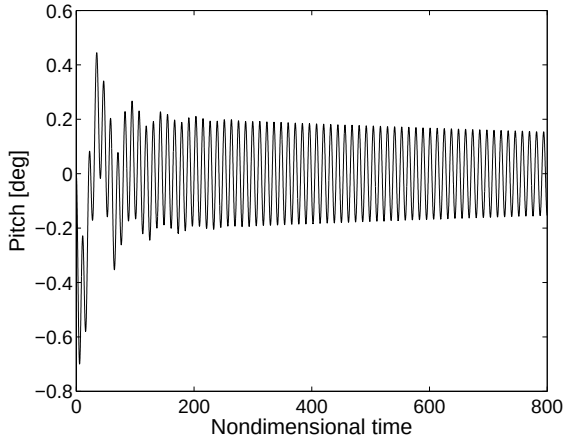

Fig. 2 Time history for linear structural model at $M = 0.86$, $\bar{U} = 3.36$ and 0.5° initial incidence.

shown in Fig. 2. The next cases consider aeroelastic behavior with initial incidences of 1.0° and -1.0°. Figures 3 and 4 show time histories with the same oscillations amplitude, *i.e.*, inicidences approximately between 0.4° and -0.4°. It is important to note that when increasing initial incidences the system also increases oscillations amplitude, for the linear structural model.

Aeroelastic responses including torsional polynomial nonlinearities in the structure have been calculated with representative nonlinear function showed in Fig. 5 and given by

$$f(\alpha) = 0.3672\alpha + 18000\alpha^3 \, . \qquad (13)$$

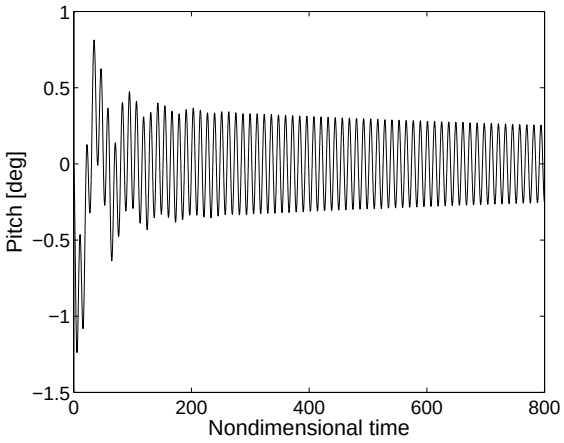

Fig. 3 Time history for linear structural model at $M = 0.86$, $\bar{U} = 3.36$ and 1.0° initial incidence.

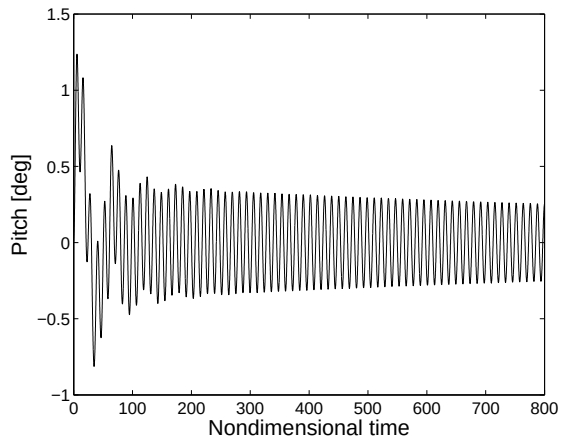

Fig. 4 Time history for linear structural model at $M = 0.86$, $\bar{U} = 3.36$ and -1.0° initial incidence.

Figure 6 depicts flutter boundaries computed using two structural models, linear and nonlinear, and two different techniques, time–marching and Hopf Bifurcation analysis. In the Hopf bifurcation case, flutter boundaries have been obtained with the structural model given by $f(\alpha) = \alpha$, *i.e.*, a linear torsional curve, and these results are represented by the diamond symbols in Fig. 6. Flutter boundaries for the nonlinear structural model given by Eq. (13), and obtained in [9], also using Hopf bifurcation analyses, are indicated by the delta symbols. However, the latter results have been obtained using only the linear portion of Eq. (13), *i.e.*, $f(\alpha) = 0.3672\alpha$ for the torsional

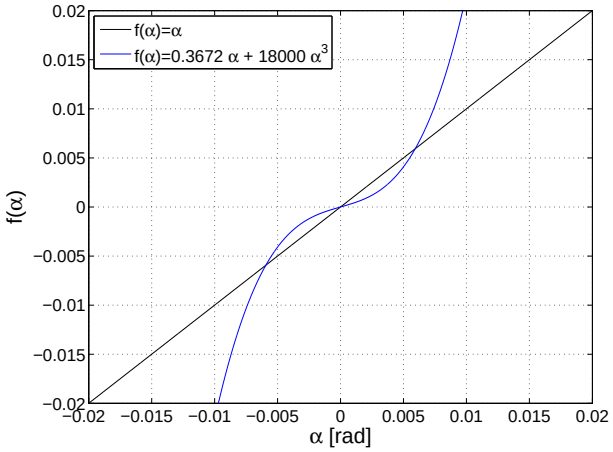

Fig. 5 Nonlinear curve $f(\alpha) = 0.3672\alpha + 18000\alpha^3$.

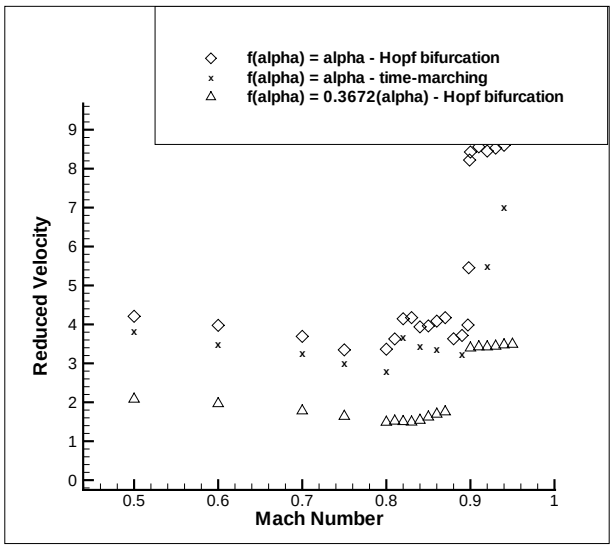

Fig. 6 Flutter boundaries.

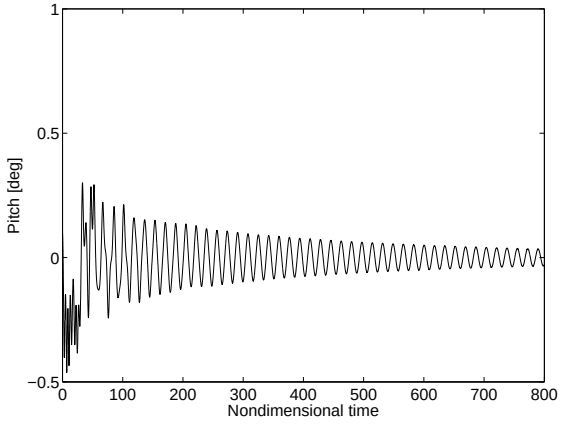

Fig. 7 Time history for nonlinear structural model at $M = 0.86$, $\bar{U} = 1.9$ and 1.0° initial incidence.

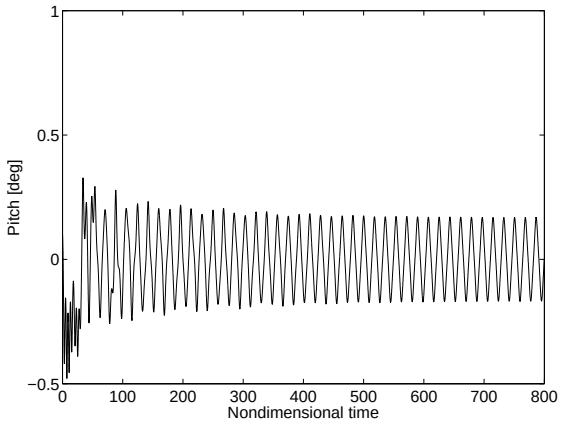

Fig. 8 Time history for nonlinear structural model at $M = 0.86$, $\bar{U} = 2.0$ and 1.0° initial incidence.

function. For instance, the nonlinear Hopf bifurcation results indicate that the flutter point for $M_\infty = 0.86$ is at $\bar{U} = 1.7$, but this value was obtained with only the linear portion of the polynomial, as reported in [9], since there is no effect of torsional nonlinear terms in the flutter speed calculations with Hopf bifurcation analysis. Time–marching flutter boundaries results for $f(\alpha) = \alpha$ torsional linear curve are also presented in Fig. 6, as in [9], for comparison purposes.

The flutter point for $M_\infty = 0.86$, considering the structural polynomial nonlinearity given in Eq. (13), is also evaluated with the time–marching methodology. Time history responses are observed with variations of $\bar{U}$, where the authors have considered 1.0° initial incidence and zero mean angle-of-attack torsional spring position ($\alpha_0 = 0$). The flutter speed of the present time-marching method is obtained when the system begins limit cycle oscillations. For instance, Fig. 7 presents the time history for $M_\infty = 0.86$ and $\bar{U} = 1.9$. In this case, the system oscillations are easily identified with converging amplitude responses. Figure 8 presents the response with small–amplitude limit cycle oscillation in pitch, indicating a nonlinear flutter point for $M_\infty = 0.86$ at $\bar{U} = 2.0$. For flight speeds above the flutter

condition, time history responses have presented limit cycle oscillation and can be observed, for $\bar{U} = 2.2$, in Fig. 12 for $M_\infty = 0.86$ and 1.0° initial incidence.

Variations of initial incidence in the time-marching method with torsional nonlinear model, given in Eq. (13), are also analyzed. Figures 9 to 13 show time histories at $M_\infty = 0.86$ and $\bar{U} = 2.2$, for different initial incidences in the calculations, namely 0.1°, 0.3°, 0.5°, 1.0° and -1.0°. Although the system exhibits different initial behavior, the motion for long times indicated LCO with the same amplitude in all cases. One can observe that time histories for 1.0° and -1.0° also exhibit different initial behavior and, after the initial transients die out, the long time behavior shows amplitude interval of oscillation from -0.2 to 0.4 for both cases, as shown in Figs. 12 and 13, respectively.

For the time-marching computations performed so far, aeroelastic response for the linear structural model has presented the same behavior with the variation of initial incidences. However, when increasing initial incidence, the system also exhibits increased oscillation amplitudes. The system with variation of initial incidences, considering the nonlinear structural model, exhibits different initial behavior, and the long time behavior indicates LCO with the same amplitude for the results with the structural parameters presented in this paper. Similar behavior can be seen in previous work [10], with the same structural model parameters but different nonlinear torsional functions. In this paper, the nonlinear torsional function, given by Eq. (13), presents a linear coefficient value larger than that from the nonlinear function curve used in [10], but the coefficients of nonlinear terms are the same. In the comparison of these solutions, different flutter speeds and different amplitudes in the responses are observed. As expected, the nonlinear function curve representing the torsional nonlinearity, given by Eq. (13), has verified the influence of the different linear coefficient values in the flutter speed and post bifurcation behavior.

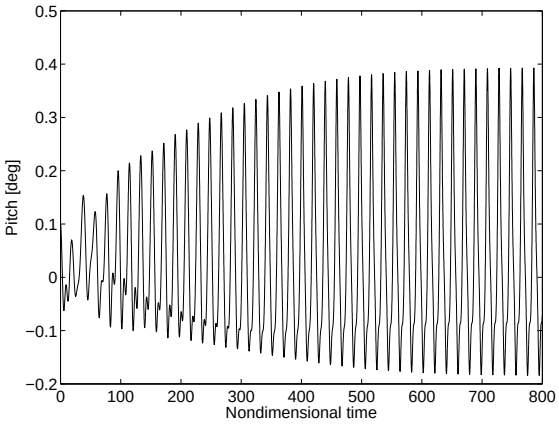

Fig. 9 Time history for nonlinear structural model at $M = 0.86$, $\bar{U} = 2.2$ and 0.1° initial incidence.

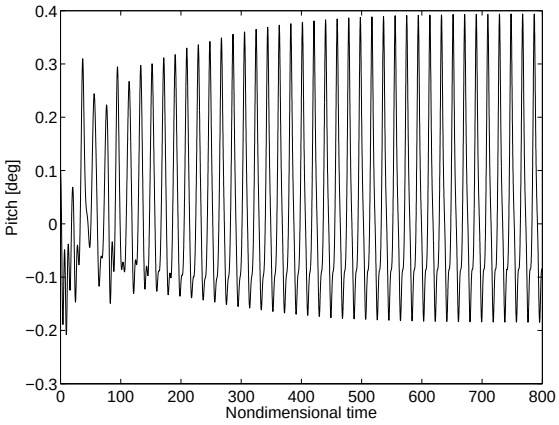

Fig. 10 Time history for nonlinear structural model at $M = 0.86$, $\bar{U} = 2.2$ and 0.3° initial incidence.

5.2 Equilibrium Angle-of-Attack Analysis

This section presents equilibrium solutions of aeroelastic system for symmetric NACA 0012 airfoil model in pitch and plunge motion. Nonzero mean angle-of-attack position (α_0) of the torsional linear and nonlinear spring is incorporated into the model for such analyses. First, equilibrium solutions of the aeroelastic model with linear structure are computed for $\alpha_0 = 1.0^\circ$ and variations in M_∞ and $\bar{U}$. Static equilibrium angle-of-attack is obtained with the time–marching methodology with variations of $\bar{U}$, below the flutter speed. Each curve of Fig. 14

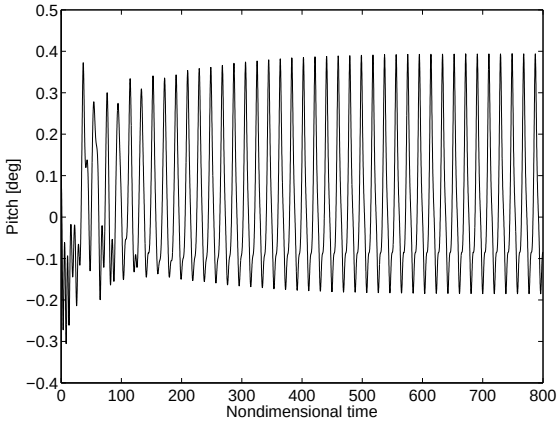

Fig. 11 Time history for nonlinear structural model at $M = 0.86$, $\bar{U} = 2.2$ and $0.5°$ initial incidence.

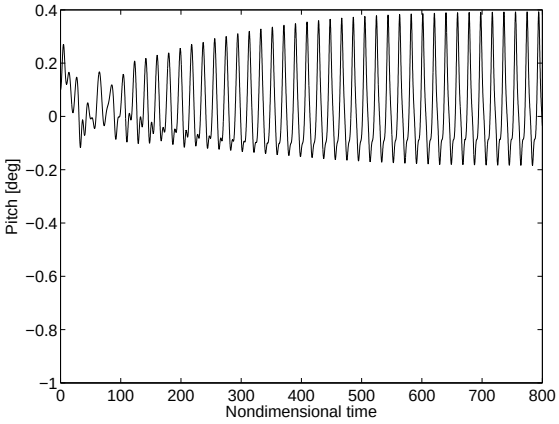

Fig. 13 Time history for nonlinear structural model at $M = 0.86$, $\bar{U} = 2.2$ and $-1.0°$ initial incidence.

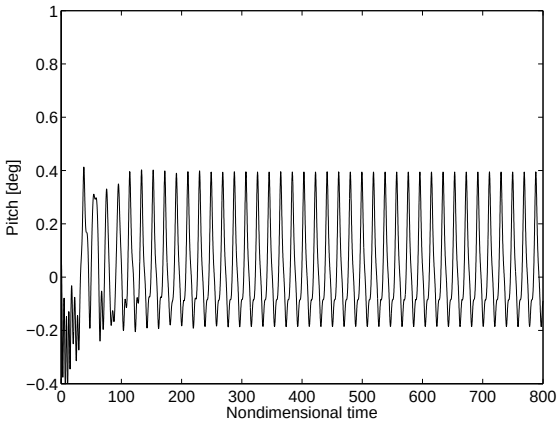

Fig. 12 Time history for nonlinear structural model at $M = 0.86$, $\bar{U} = 2.2$ and $1.0°$ initial incidence.

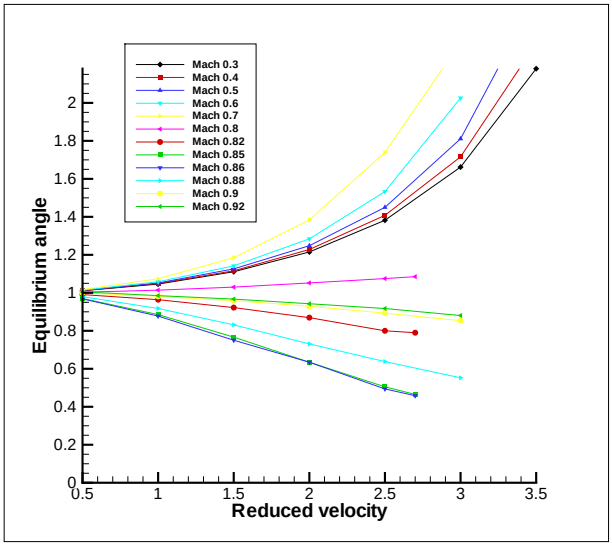

Fig. 14 Equilibrium angle-of-attack for linear structural model ($f(\alpha) = \alpha$): $\alpha_0 = 1.0°$ and $1.5°$ initial incidence.

presents equilibrium angle-of-attack α_{eq} position versus $\bar{U}$ at fixed Mach number.

A variation of Mach number from 0.3 to 0.92 has presented different equilibrium positions in the solutions, as shown in Fig. 14. Increasing small variation in α_{eq} is observed from $M_\infty = 0.3$ to $M_\infty = 0.7$, for the same $\bar{U}$ values. These freestream Mach numbers produce subsonic flow throughout the domain for $\alpha_0 = 1.0°$. The trend of increasing α_{eq} with increasing $\bar{U}$ is maintained for each subsonic Mach number. When the flowfield Mach number increases over $M_\infty = 0.7$, the equilibrium angle of attack starts to decrease with the increase in the reduced velocity, as observed in the equilibrium angle-of-attack positions from $M_\infty = 0.8$ to $M_\infty = 0.86$. This reversal in trend is observed in the transonic flight regime. Furthermore, for $M_\infty = 0.88$, $M_\infty = 0.9$ and $M_\infty = 0.92$, and at a fixed $\bar{U}$, it is observed that the equilibrium angle-of-attack increases as the freestream Mach number increases, as one can see in Fig. 14.

Equilibrium solutions of the aeroelastic system with nonlinear structural model are also computed for the nonlinear torsional curve given by

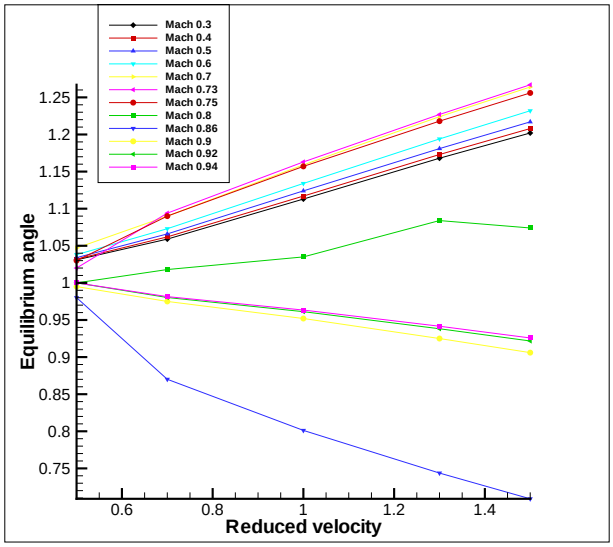

Fig. 15 Equilibrium angle-of-attack for nonlinear structural model ($f(\alpha) = 0.3672\alpha + 18000\alpha^3$): $\alpha_0 = 1.0^\circ$ and 1.5° initial incidence.

Eq. (13). The results for $\alpha_0 = 1.0^\circ$ and variations of M_∞ and $\bar{U}$ are shown in Fig. 15. Again, the static equilibrium angle-of-attack is obtained with the time–marching methodology with variations of $\bar{U}$ below the flutter speed. As before, an increasing trend in α_{eq}, but with very small variations, is observed from $M_\infty = 0.3$ to $M_\infty = 0.73$, at fixed $\bar{U}$. As one starts to have transonic flowfield conditions, the equilibrium angle-of-attack values start to decrease, as in the previous study. Again, as observed in the previous cases, α_{eq} still decreases with the increase in $\bar{U}$, but, for a fixed $\bar{U}$, results indicate smaller α_{eq} values as the Mach number increases.

For comparison purposes, results for the calculations at $M_\infty = 0.86$, $\bar{U} = 1.5$ and $\alpha_0 = 1.0^\circ$, shown in Figs. 14 and 15, are also presented in Table 2. As previously discussed in the present work, linear and nonlinear structural models have obtained similar equilibrium angle-of-attack behavior with variations of the freestream Mach number. However, equilibrium angle-of-attack positions considering linear and nonlinear structural models for the same variations of M_∞ have presented different values.

Table 2 Equilibrium angle for $\bar{U} = 1.5$.

Mach number	Eq. angle ($f(\alpha) = \alpha$)	Eq. angle (Eq. (13))
0.3	1.1110	1.2020
0.4	1.1160	1.2080
0.5	1.1260	1.2170
0.6	1.1420	1.2320
0.7	1.1850	1.2640
0.8	1.0300	1.0740
0.86	0.7503	0.7090
0.9	0.9589	0.9060
0.92	0.9670	0.9217

Concluding Remarks

Time-marching analyses are compared to direct calculations of Hopf bifurcation points for linear and nonlinear structural case presented in [9], where the results agree well. Torsional polynomial nonlinearities considered in the present work have shown significant effects on the aeroelastic responses and that yield limit cycle oscillations can occur below the linear flutter speed. For the time-marching computations performed, aeroelastic responses for the linear structural model have presented the same behavior with the variation of initial incidences. However, when increasing the initial incidences, the system also exhibits increased oscillation amplitudes. Aeroelastic responses of the nonlinear structural models, with increasing initial incidences, have presented limit cycle oscillation with the same interval amplitude.

Finally, equilibrium angle-of-attack positions with variations of Mach number and reduced velocity for $\alpha_0 = 1.0^\circ$ have indicated different values. Subsonic flowfield Mach numbers have increasing α_{eq}, while at transonic flowfield conditions the NACA 0012 airfoil pitches down to a new equilibrium position, considering linear and nonlinear structural model. However, linear and nonlinear structural model responses have obtained different equilibrium angle-of-attack positions for the same variations of Mach number and

at fixed $\bar{U}$.

6 Acknowledgements

The authors gratefully acknowledge the partial support for this research provided by Conselho Nacional de Desenvolvimento Científico e Tecnológico, CNPq, the Integrated Project Research Grant No. 312064/2006-3. The authors also gratefully acknowledge the very productive interaction with Prof. Ken Badcock and Dr. M. Woodgate, who provided the Hopf bifurcation code used in the present research.

References

[1] Bisplinghoff, R. L., Ashley, H., and Halfman, R. L., "*Aeroelasticity*", Addison-Wesley, Cambridge, MA, 1955.

[2] Lee, B. H. K., and Price, S. J. and Wong, Y. S., "Nonlinear aeroelastic analysis of airfoils: bifurcation and chaos", *Progress in Aerospace Sciences*, Vol. 35, 1999, pp. 205-334.

[3] Morton, S. A., "Nonlinear analysis of airfoil flutter at transonic speeds", PhD Thesis - School of Engineering of the Air Force Institute of Technology, OH, USA, May 1996.

[4] Badcock, K. J.; Woodgate, M. A.; Richards, B. E., "Hopf bifurcation calculations for simmetric airfoil in transonic flow", *AIAA Journal*, Vol. 42, No. 5, May 2004, pp. 883-892.

[5] Badcock, K.J., Woodgate, M.A., and Richards, B.E., "Direct Aeroelastic Bifurcation Analysis of a Simmetric Wing Based on Euler Equations", *Journal of Aircraft*, Vol. 42, No. 3, May-June 2005.

[6] Alonso, J. J., and Jameson, A., "Fully-implicit time-marching aeroelastic solutions", *Proceedings of the 32nd AIAA Aerospace Sciences Meeting & Exhibit*, Reno, NV, Jan. 1994.

[7] Camilo, E., Marques, F. D., and Azevedo, J. L. F., "Dynamic analysis of aeroelastic response for transonic flow with nonlinear structural model", *Proceedings of the 26th International Council of the Aeronautical Sciences – ICAS 2008*, Alaska, USA, 2008.

[8] Kousen, K. A., and Bendiksen, O. O., "Limit cycle phenomena in computational transonic aeroelasticity", *Journal of Aircraft*, Vol. 32, No. 2, 1994, pp. 1257-1263.

[9] Camilo, E., Marques, F. D., and Azevedo, J. L. F., "Hopf bifurcation analysis of typical sections with structural nonlinearities in transonic flow", AIAA Paper No. 2008-6236, *Proceedings of the 26th AIAA Applied Aerodynamics Conference and Exhibit*, Honolulu, Hawaii, 2008.

[10] Camilo, E., Azevedo, J. L. F., and Marques, F. D., "Nonlinear behavior of typical airfoil sections in the transonic regime", *Proceedings of the 30th Ibero–Latin–American Congress on Computational Methods in Engineering – CILAMCE 2009*, Armação dos Búzios, Rio de Janeiro, Brazil, 2009.

[11] Azevedo, J.L.F., "On the development of unstructured grid finite volume solvers for high speed flows", Report NT-075-ASE-N/92, Instituto de Aeronáutica e Espaço, São José dos Campos, SP, 1992.

[12] Simões, C. F. C., and Azevedo, J. L. F., "The influence of numerical parameters on unsteady airfoil inviscid flow simulations using unstructured dynamic meshes", *Proceedings of the 15th Brazilian Progress in Aeroespace Engineering – COBEM 99*, Águas de Lindóia, São Paulo, Brazil, 1999.

[13] Bigarella, E. D. V., and Azevedo, J. L. F., "A Study of convective flux computation schemes for aerodynamic flows", AIAA Paper No. 2005-0633, *Proceedings of the 43rd AIAA Aerospace Sciences Meeting and Exhibit*, Reno, NV, 2005.

[14] Bigarella, E. D. V., and Azevedo, J. L. F., "Advanced eddy-viscosity and reynolds-stress turbulence model simulations of aerospace applications", *AIAA Journal*, Vol. 45, No. 10, 2007, pp. 2369-2390.

[15] Oliveira, L. C., "A state-space aeroelastic analysis methodology using computational aerodynamics techniques", Master Thesis - Instituto Tecnológico de Aeronáutica, São José dos Campos, S. P., Brazil, 1993 (in Portuguese).

[16] Marques, A. N., and Azevedo, J. L. F., "Unsteady aerodynamic forces for aeroelastic analysis of two-dimensional lifting surfaces", *Journal of the Brazilian Society of Mechanical Sciences and Engineering*, Vol. 28, 2006, pp. 474-484.

[17] Marques, A. N., and Azevedo, J. L. F., "A

z-transform discrete-time state-space formulation for aeroelastic stability analysis", *Journal of Aircraft*, Vol. 45, No. 5, Sept.-Oct. 2008, pp. 1564-1578.

[18] Jameson, A., Schmidt, W., and Turkel, E., "Numerical simulation of the Euler equations by finite volume using Runge-Kutta time stepping schemes", AIAA Paper No. 81-1259, 1981.

6.1 Copyright Statement